Radial evolution of the properties of small-scale magnetic flux ropes in the solar wind

Journal of Physics: Conference Series **1332** (2019) 012005 doi:10.1088/1742-6596/1332/1/012005

Radial evolution of the properties of small-scale magnetic flux ropes in the solar wind

Qiang Hu, Yu Chen, and Jakobus le Roux

Department of Space Science and CSPAR, The University of Alabama in Huntsville, Huntsville, AL 35805, USA

E-mail: qiang.hu@uah.edu

Abstract. Small-scale magnetic flux ropes, most with duration $\leq$ 1 hour at 1 AU, are found to be ubiquitous in the solar wind from in-situ spacecraft measurements. We have built an event database (fluxrope.info) for these structures identified and summarized their main physical properties. Quantitative analysis provided strong evidence in support of the view of their generation through turbulence cascade processes in space plasmas. We extend such analysis to spacecraft measurements at larger radial distances, mainly those from the Ulysses spacecraft mission. We perform comparison of relevant properties of these structures and reveal their radial evolution near the ecliptic plane. Meanwhile we also try to derive, quantitatively, the parameters important for the underlying processes including magnetic reconnection, intrinsic to turbulence cascade, in order to aid in relevant theoretical investigations. We also supplement the largely statistical analysis results with individual case studies to illustrate the process of flux rope merging and associated particle energization signatures through an observational approach. We speculate on the implications of our results and foresee future investigations that can help improve our current understanding of the origin and evolution of these small-scale magnetic flux ropes throughout the heliosphere.

1. Introduction

Small-scale magnetic flux ropes, usually identified from in-situ spacecraft measurements with duration ranging from tens of minutes to a few hours, constitute an important type of space plasma structures. They are found to be present in interplanetary medium, embedded in solar wind streams, especially near the heliospheric current sheet (HCS) in the ecliptic plane [1, 2, 3, 4, 5, 6]. They arguably can go further down to even smaller scales, e.g., to duration of a few seconds, provided that the cadences of in-situ measurements for both magnetic field and plasma parameters are sufficiently high. For more sophisticated analysis and modeling approaches, employing the in-situ spacecraft data, both data sets are needed to achieve a more general characterization of the flux rope structures in both their configurations and physical properties, especially in a highly quantitative manner. In addition, auxiliary but increasingly available measurements on suprathermal electrons and elemental composition/charge states are also desirable for discerning the characteristics of the underlying structures and the associated interpretation of their origin [7, 8].

One method that distinguishes itself from the others is the so-called Grad-Shafranov (GS) reconstruction technique, based on the Grad-Shafranov equation describing a two-dimensional (2D) plasma configuration in magnetohydrostatic equilibrium. The main advantage of the GS

reconstruction is the full characterization of the 2D configuration in cylindrical geometry by a single scalar function, A, which represents the nested magnetic flux surfaces enclosing a central cylindrical axis for a flux rope configuration. This enables the reconstruction of the distribution of the flux function over the cross section plane, given the measured values along the spacecraft path across the nested flux surfaces. The standard output from the GS reconstruction includes the geometric parameters of the structure, namely, the cylindrical axis orientation as well as the spatial extent of the cross section, and the set of physical quantities characterizing the magnetic field configuration by yielding the spatial distributions of magnetic field components and other derived quantities such as the current density.

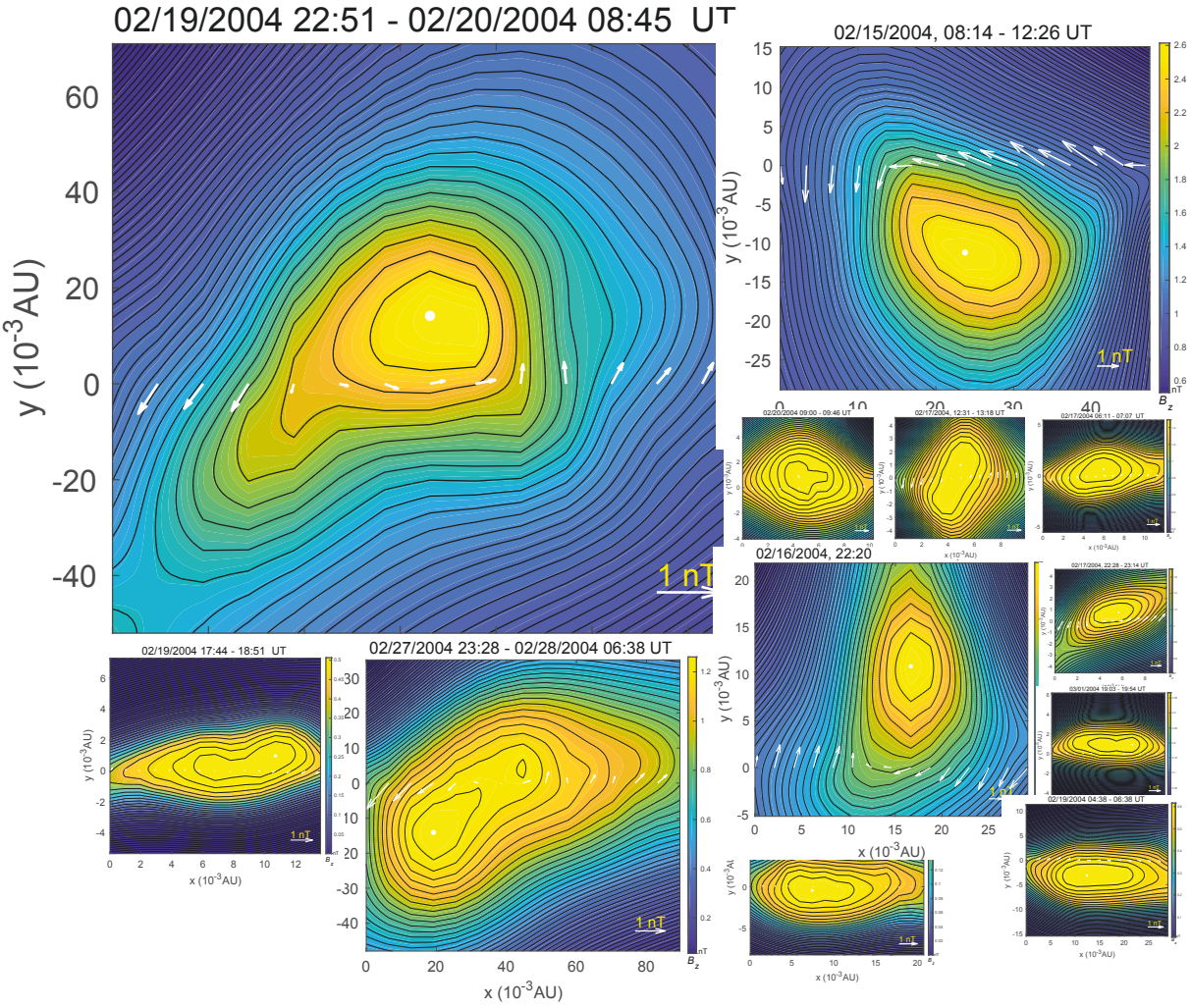

Figure 1. A collage of cross sections of cylindrical flux ropes obtained from the quantitative GS reconstruction results (approximately to scale; adapted from [9]). Each rectangle represents a spatial domain over the cross section of the flux rope, on a plane perpendicular to its cylindrical axis with contours of the magnetic flux function A (equivalent to the transverse field lines) and the axial field component in color. See Figure 8 for detailed descriptions of flux rope configuration from GS reconstruction result. The center usually possesses the strongest axial field. Note the axis orientation varies from one flux rope to the other.

The procedures of the GS reconstruction have been well established and applied to various

space plasma environment. We refer the readers to a recent technical review [10] for details. Recent development most relevant to this report is the implementation of the GS-based automated detection algorithm of small-scale magnetic flux ropes with demonstrated success [4, 11]. An unprecedented number of events with significant amount of variability is identified and archived, which has enabled meaningful statistical analysis and pursuit of inter-connections to other relevant studies. The technical details of the implementation are provided in a recent publication [4], documenting the database built based on this approach. As an ongoing effort, the identification and characterization of small-scale magnetic flux ropes are carried out for various spacecraft missions. The results, in the form of event lists with a set of concise but essential information, are summarized and archived on the event database website, `https://fluxrope.info`.

To get a glimpse into the capability of the GS reconstruction technique and the wealth of information it generates, we show, in Figure 1, an example of a collection of selected flux rope configurations obtained from the Ulysses spacecraft in-situ measurements at a heliocentric distance ~ 5 AU over a time period of about two weeks. These are the actual GS reconstruction output for a dozen data intervals (adapted from [9]), showing the cross section configurations typical of magnetic flux ropes with nested flux surfaces on which the field lines are winding around the central axis (owing to the non-vanishing axial field component). Despite such a common flux rope configuration, they show great variability in overall shape, scale size and other properties. Here the scale sizes, approximately to scale as illustrated, vary from about 0.01 AU to 0.1 AU. Generally the distributions of their duration and scale sizes exhibit power laws, based on the statistical analysis of our database, containing tens of thousands of events [4, 6], with more numbers of events with smaller values. Whether there exists a smooth transition to or an indication for a distinct population of the large-scale flux ropes (with duration of tens of hours to days, i.e., the magnetic clouds) remains unclear, partially due to the relatively small event counts for that range. It is interesting to note that although these flux ropes differ in their axial orientations, there does exist a general trend for the flux rope axes to align with the local Parker spiral direction, especially for events occurring near the ecliptic plane [4, 6].

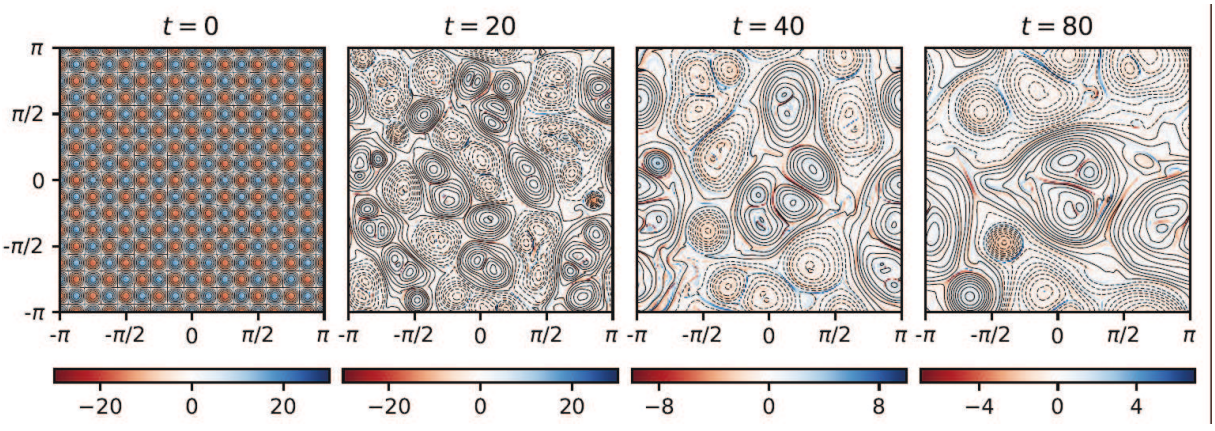

Figure 2. The numerical simulation for the evolution of 2D flux rope merging process from $t = 0$ with idealized distribution of flux ropes with equal sizes and alternating signs of helicity. The contours represent the magnetic flux function ψ and the colors the (axial) current density (adapted from [12]).

One benefit of the GS reconstruction technique is to enable a direct comparison of the physical quantities with the corresponding numerical simulation results. For example, the GS output of

the 2D magnetic flux function A and the axial field and current density (j_z, also a function of A) corresponds to the dependent variables employed in many 2D magnetohydrodynamic (MHD) simulations of turbulence [13, 14, 15, 16]. As an example, Figure 2 [12] illustrates exactly the same physical quantities as in Figure 1 for a 2D MHD simulation of inverse cascade process. These physical quantities have direct one-to-one correspondence to the GS reconstruction output, i.e., $A \equiv \psi$. Therefore a direct and physical connection can be made between the two realms. One testament to this approach is a recent study by Zheng and Hu [11] in which a direct comparison between the distributions of the axial current density in flux rope/island structures from the GS-based observational analysis and 2D MHD simulations was made to demonstrate the non-Gaussian features present in both results. Such a study provided observational evidence for the view of the correspondence of these structures to 2D MHD turbulence in the inertia range [17, 18]. We will further pursue this type of investigation by comparing our observational result with the numerical simulation study of [12] in Section 2.2.

Motivated by these recent development, we have expanded the ongoing analysis to additional spacecraft missions. In Section 2, we present a comparison of a set of selected properties for flux ropes identified at two separate ranges of heliocentric radial distances near the ecliptic plane. We explore the possible underlying mechanism responsible for the radial evolution of these properties, in the context of flux rope merging (inverse cascade), a scenario depicted in Figure 2. We then attempt to zoom in and focus on one particular case study, hinting at flux rope merging between two adjacent flux ropes. We will present a few key characteristics including associated energetic particle signatures. Lastly, we conclude and offer some additional thoughts in the last section.

2. Radial Dependence of Flux Rope Properties

Table 1. Radially distributed flux rope events from ACE and Ulysses spacecraft.

Database	Latitudes	Radial Distances	Walén test slope	Event Counts
ACE	0°	1 AU	≤ 0.3	17,602
Ulysses	$< 30°$	>3.5 AU	≤ 0.5	10,124

We have applied the automated detection algorithm to a number of spacecraft missions and established small-scale flux rope databases with significant number of events. A unique database is from the Ulysses mission which had a unique polar orbit over the poles of the Sun that covered a wide range of heliographic latitudes and heliocentric radial distances (from ∼1 to 5 AU). We describe here briefly a subset of events from the Ulysses database corresponding to the events detected in low latitudes, but at larger radial distances beyond 3.5 AU, and compare with the corresponding results detected at 1 AU. For a comprehensive report on all the events detected throughout the entire Ulysses mission, see Chen et al. [6].

2.1. Comparison Between ACE and Ulysses Results

We specifically focus on the radial evolution of flux rope properties by utilizing the simultaneous flux rope detection results at 1 AU from the ACE spacecraft for the time periods, 1998-02-05∼1999-07-14, and 2002-10-12∼2005-09-14, when Ulysses was spending extensive periods of time near the ecliptic plane. To better facilitate the inter-comparison between ACE and Ulysses, we use exactly the same duration range, $9 \sim 2165$ minutes, for the flux rope intervals contained in the two event sets. The different conditions and search criteria are summarized in Table 1. The different Walén test slopes have little impact on the search result, since reducing the slope to 0.3 for Ulysses results in very little change in the detection rate [6].

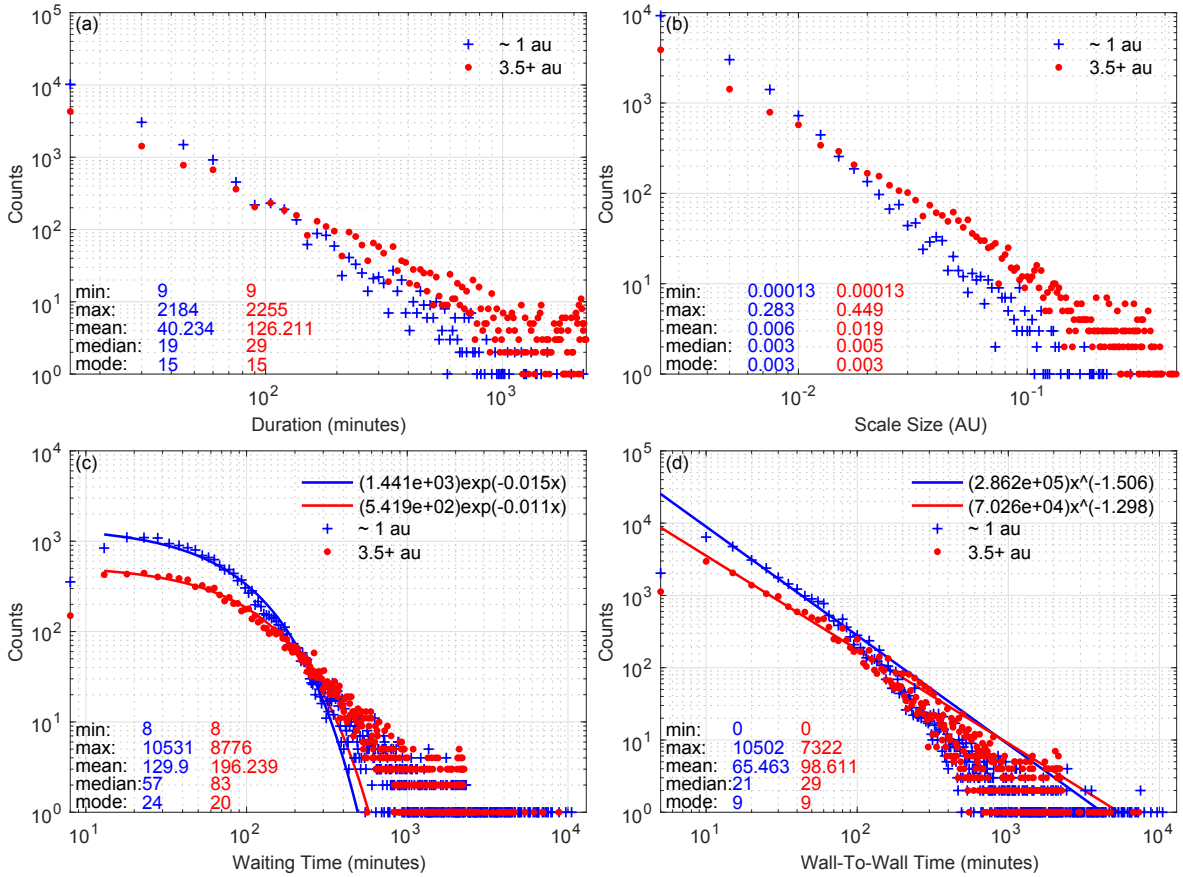

Figure 3. The distributions of flux rope properties for the radially aligned events from ACE and Ulysses. These properties are (a) duration, (b) scale size, (c) waiting time, and (d) wall-to-wall time. In (c) and (d), the exponential and power-law fitting curves are drawn for the lower-range property values with the fitting parameters denoted.

There is a clear decrease in the number of event counts from a radial distance at 1 AU to increased distances, for the same time periods and the same range of duration. When comparing the two event sets, there are clear discrepancies in plasma and magnetic field parameters, simply due to the radial evolution of solar wind plasmas, in terms of radially decaying plasma density, temperature, and magnetic field magnitude (not shown). For the other selected flux rope properties, shown in Figure 3, the difference is seen in the overall distributions from the two sets. For the distributions of duration and scale size, they exhibit clear power laws, but possess different power-law indices. For the distribution of waiting time, defined as the elapsed time between the beginning times of two adjacent flux rope intervals, an exponential functional seems to fit each distribution well for the smaller value portion, but with different fitting parameters. Figure 3d shows the wall-to-wall time distribution, which is considered to be equivalent to the waiting time distribution of current sheets near the flux rope boundaries [11]. They were found to be power-law like in the lower-value range below certain break point, corresponding to the correlation length scale of the MHD turbulence in the inertial range [14]. The power-law fittings are given, respectively, for the two distributions at different radial distances. The power-law indices are different and the break points are different as well with one around ~ 80 minutes for the distribution at 1 AU and the other ≥ 200 minutes, respectively.

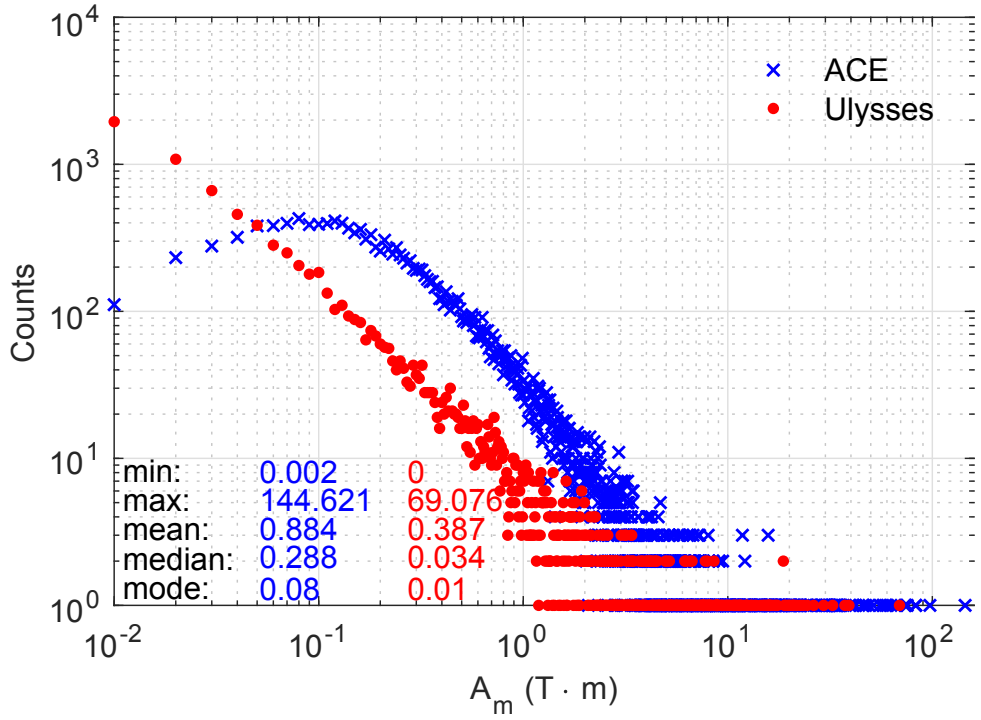

Figure 4. The distributions of the poloidal magnetic flux A_m for both ACE and Ulysses event sets.

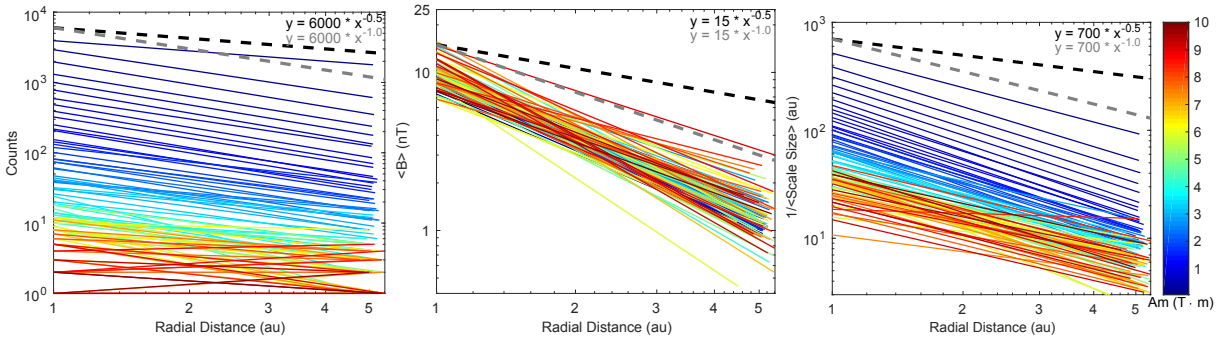

Figure 5. The radial variations of the number of event counts N, the average field magnitude $\langle B \rangle$, and the inverse scale size k (from left to right panels) in log-log scales, respectively. Each colored line connects the values at ACE and Ulysses, corresponding to the events with approximately the same A_m as indicated by the colorbar. The dashed lines provide the guide lines with power-law slopes -1 and -0.5, respectively.

2.2. Radial Evolution Owing to Flux Rope Merging

We attempt to examine the possible radial evolution of flux rope properties, making use of the databases obtained from ACE and Ulysses spacecraft. Although the flux ropes could be primarily generated through local processes independently at different radial distances, one possible scenario is the evolution of these structures in time due to interactions while convecting with the solar wind. Owing to the process of merging between adjacent flux ropes, this will

lead to the corresponding radial evolution that may be present in our databases. One such process was proposed and studied by numerical simulations, considering the successive merging between adjacent flux ropes, as illustrated in Figure 2 [12]. The temporal evolution depicted corresponds to an inverse cascade process intrinsic to 2D MHD turbulence, resulting in larger scale size flux ropes with decaying magnetic field strength and fewer counts when time progresses. Based on simple "hierarchical merging" argument and the principle of (poloidal) magnetic flux conservation during flux rope merging (see also [19]), a number of scaling laws with respect to time t is deduced for the event counts N, the average field magnitude $\langle B \rangle$, and the inverse scale size k [12]:

$$N \sim t^{-1}, \quad \langle B \rangle \sim t^{-0.5}, \quad k \sim t^{-0.5},$$

under the condition that the poloidal magnetic flux $\psi(t) = \psi(0)$ is conserved for each flux rope.

From our observational point of view, we can translate t into the radial distance r, and obtain the aforementioned quantities from our databases at discrete radial distances (only two at the present time). Then we bin them according to the corresponding poloidal flux content in each flux rope, complying with the condition of flux conservation. Figure 4 shows the distributions of the amount of the poloidal magnetic flux, $A_m \equiv \psi$, representing the absolute extreme value in A with the flux rope boundary defined with $A_b \approx 0$. The range of A_m for both event sets is $[0.05, 10]$ T·m, excluding the greater values corresponding to the large-scale flux ropes which may have clear solar origin. Then we bin the three quantities for all the events based on their corresponding A_m value, and present each bin containing two points at two separate radial distances, in Figure 5. Therefore each bin (colored line) represents the radial change in the corresponding quantity subject to the possible merging process discussed above. It is seen that in general these quantities all decay with r and with power-law indices close to -1, or somewhere in-between -0.5 and -1 at best, not strictly following the prediction of [12]. Of course one caveat is that we only have two distinct points in r. It would be desirable to extend the analysis to more datasets at additional radial distances.

3. Flux Rope Merging: A Case Study

It is also informative to pursue in the direction of individual case study, from the perspective of detailed and quantitative characterization of flux rope merging between a pair of adjacent flux ropes, via the approach of GS reconstruction. We present one such case observed by both the ACE and Wind spacecraft in March 1999 when they were separated by about 250 Earth radii mostly along the Sun-Earth line. Therefore the same solar wind streams passed both spacecraft with a time delay of about an hour with ACE being further upstream.

Figure 6 shows the time series of the solar wind magnetic field and plasma parameters, together with the energetic ions flux (the bottom panel) from ACE. A number of flux ropes was identified downstream of the interplanetary shock, at 00:40 UT as marked by the vertical line. The flux rope intervals are shaded and numbered in numeric order. The intervals denoted "7" and "8" are of interest and are taken for a GS reconstruction study, partially for the reason of simultaneous ions flux enhancement, especially in the energy range $\sim$ 50 - 200 keV. The same set of measurements for the corresponding time period from Wind spacecraft is shown in Figure 7, where the flux rope interval "7" is believed to correspond to the adjacent intervals "7" and "8" in Figure 6. Such a coincidence of radial correspondence can be justified by the timing analysis of similar structures between ACE and Wind. For example, the preceding shock, the similar high-speed stream downstream, the similar magnetic field profiles during those flux rope intervals, and particularly the distinct features of the discontinuities bounding the flux rope intervals are all present in both measurements. They all seem to be consistent with a rapid transit ($\sim$ 1 hour) of these structures between the two spacecraft.

The corresponding GS reconstruction results of the cross section maps for both ACE and Wind intervals are shown in Figure 8, approximately to scale. From the ACE 2D cross

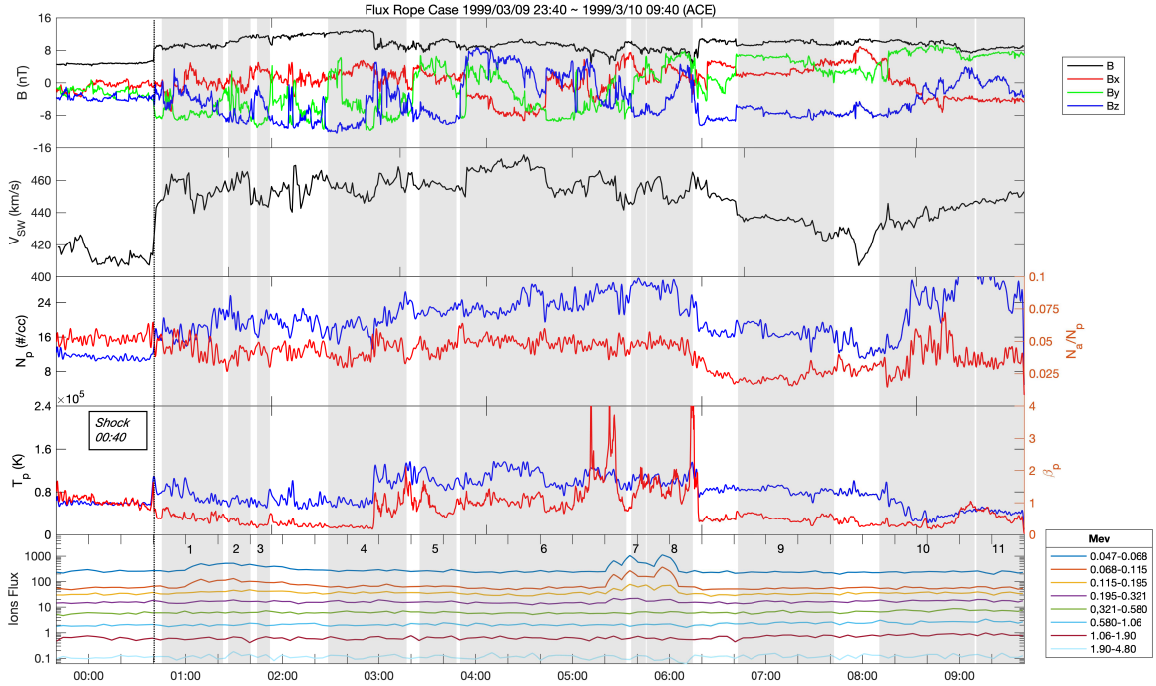

Figure 6. The time-series data from ACE spacecraft for the time period (in UT) noted on top. The panels, from top to bottom, are the magnetic field magnitude and components, the solar wind speed, the proton number density (left axis) and the alpha particle to proton number density ratio (right axis), the proton temperature (left axis) and proton β (right axis), and the ion fluxes with the corresponding energy channels shown to the right. The vertical line marks the passage of an interplanetary shock. Shaded areas represent identified flux rope intervals and are numbered.

section map, there exist two sets of cylindrical flux surfaces with parallel axes, undergoing reconnection and forming an X-point (X-line extending in the z dimension). From the Wind result, corresponding to about 1 hour later in time, a single set of nested flux surfaces emerges, centering around a central axis. Although each map is considered a snapshot of the quasi-static structure not varying in time, the morphology of the field configuration represented by these two maps obtained from real data at two closely separated times hints at the possible merging process due to the magnetic field topology favorable for magnetic reconnection. This result provides a unique and quantitative proof of such a process, provided that the dynamic evolution time scale is much longer than the transit time of the structure across the observing platforms.

For this to be satisfied in the current case, the dynamic evolution time may need to be in the order of 10^4 seconds, which can be considered to be the time taken for the two flux ropes to fully merge via magnetic reconnection. Thus the reconnected magnetic flux during the process would be equal to the amount of the poloidal flux involved. If we take the typical value 1 T·m, then the time τ it takes for the complete merging process is related to the reconnection rate or the reconnection electric field E_r via $\tau \approx 1/E_r$. For $\tau = 10^4$ seconds, the reconnection rate is approximately 10^{-4} V/m or 0.1 mV/m, which is not unreasonable for the solar wind, given that a value on the order of 1 mV/m was typically found for the reconnection events at the Earth's magnetopause [21].

Table 2 lists the physical parameters deemed important for the merging process, which has yet

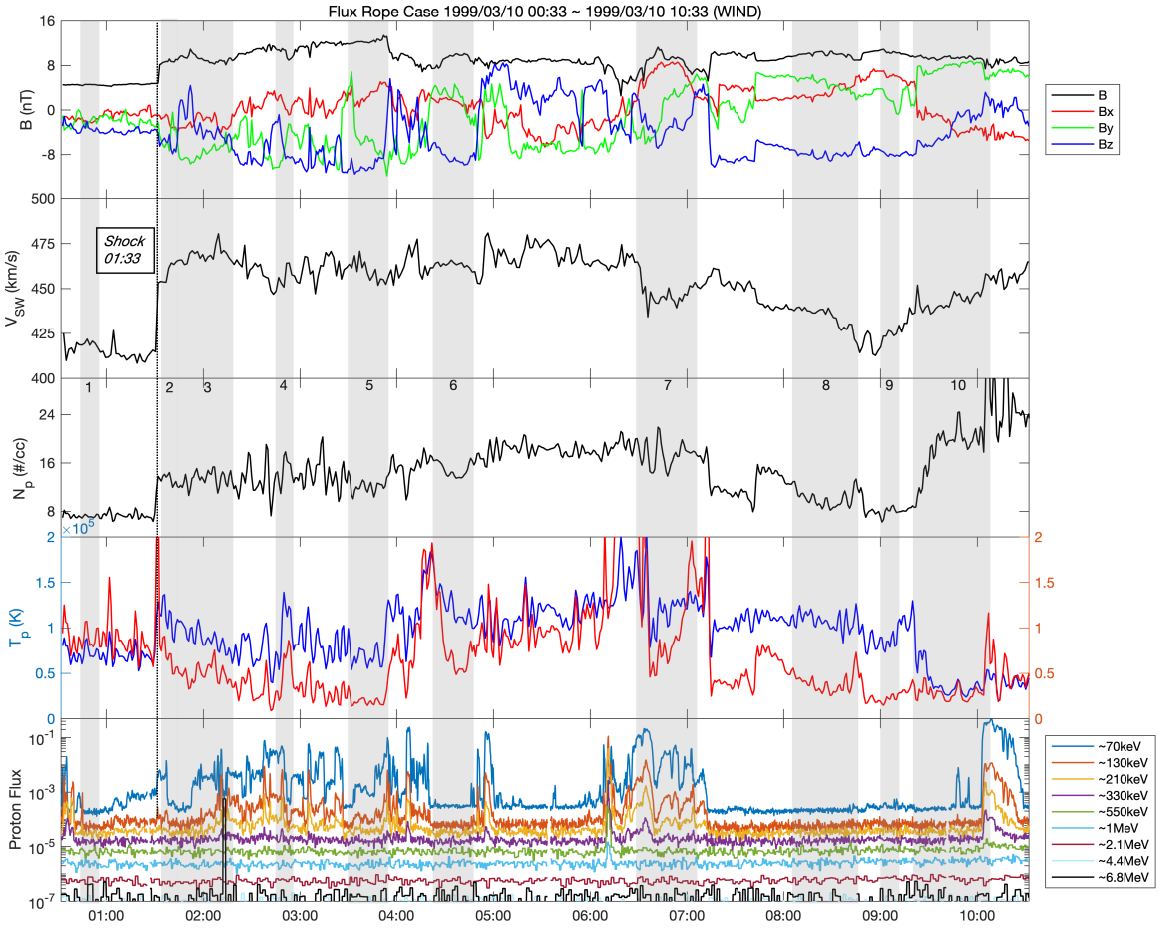

Figure 7. The time-series data from Wind spacecraft for the time period (in UT) noted on top. The format is the same as Figure 6.

Table 2. Main flux rope parameters of the GS reconstruction results from ACE (second row) and Wind (third row) spacecraft for the March 10, 1999 case study.

Φ_p (T·m)	$\Phi_t(10^9$ Wb)	B_{z0} (nT)	$j_{z0}(10^{-11}$ A/m^2)	$I_z(10^9$ A)
1.68	2.68	8.4	-4.7	-0.014
1.78	2.48	9.9	-4.5	-0.010

to be better related to theoretical investigations. The amount of poloidal flux (per unit length) Φ_p is nearly identical for the two spacecraft, corresponding to the values at the beginning or in the middle, and at the end of the merging process, respectively. The other values, including the toroidal flux Φ_t, the maximum axial field B_{z0}, the maximum axial current density j_{z0}, and the total current I_z, are typical for the flux rope of such a scale size.

4. Conclusions and Discussion

In conclusions, we have applied the automated flux rope detection algorithm based on the GS reconstruction to a number of in-situ spacecraft missions in the solar wind, and generated event databases with the event occurrence rates of a few hundreds per month on average [4, 6]. In

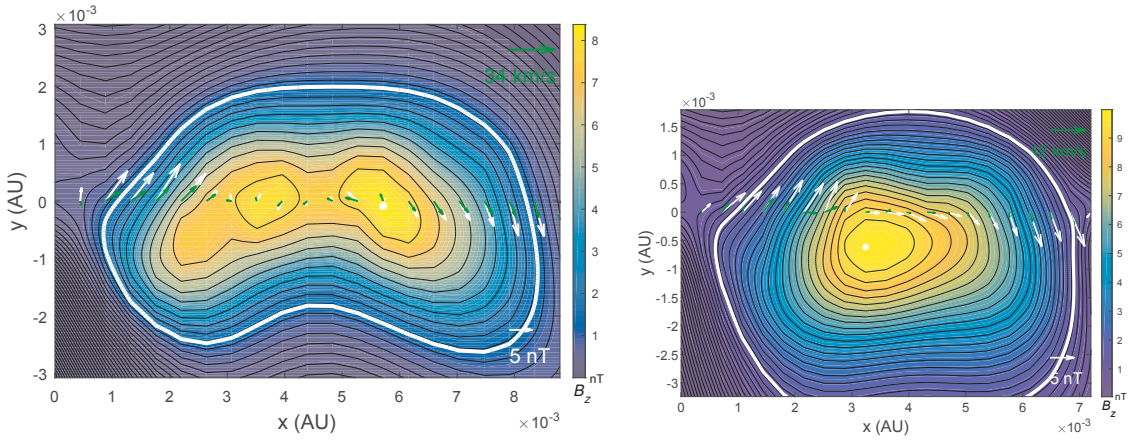

Figure 8. The GS reconstruction result of the cross sections of the flux rope from ACE (left panel) and Wind (right panel) spacecraft measurements, respectively. On each cross section map, the black contours represent the iso-surfaces of the magnetic flux function and the colors the axial magnetic field component with scales given by the colorbar in nT. The white arrows are the measured transverse field components along the spacecraft path ($y = 0$), while the green arrows the corresponding remaining transverse plasma flows in the frame moving with the structure. Two reference arrows of the magnitude "5 nT" and the local average Alfvén speed are drawn to scale for the transverse magnetic field magnitude and remaining flow speed, respectively. The thick white contour line marks the flux rope boundary [20].

particular, we have extended our analysis to the in-situ measurements by the Ulysses mission at the heliocentric radial distances greater than 1 AU, near the ecliptic plane, and compared with the corresponding analysis result at 1 AU.

We find that the main flux rope properties such as the duration, scale size and wall-to-wall time all follow power-law distributions, but possess different power-law indices for the event sets at different radial distances. The waiting time distributions, on the other hand, exhibit the exponential function behavior with different exponents. The wall-to-wall time distribution for the event set from Ulysses at greater radial distances exhibits a break point at ~ 200 minutes. A preliminary analysis on the radial evolution of selected flux rope properties including the event count, the average magnetic field, and the inverse scale size does not yield the scaling laws with respect to the radial distance, predicted by a simple "hierarchical merging" argument, albeit it should be cautioned that only two distinct radial distances are considered. A detailed case study is performed for the flux rope intervals traversed by the radially aligned ACE and Wind spacecraft. The reconstructed cross-section maps of the flux function at the two spacecraft locations / instances (about 1 hour apart) reveal the presumed merging process, i.e., a pair of adjacent single flux ropes at ACE becoming one single flux rope at Wind. During the process, it is also found that the poloidal magnetic flux is conserved, a quantitative result envisaged by some theoretical works. There are also simultaneous energetic ions flux enhancement coinciding with the flux rope intervals. The implications of these coincident or co-spatial signatures have yet to be explored, especially in a more quantitative manner.

Motivated by the recent development in theoretical investigations of particle energization by flux rope dynamics including merging (e.g., [22]), it is also attempting to try to correlate the topological change revealed for the flux rope merging, in this study, to the associated particle signatures. However it is still challenging to make direct comparisons, considering the disparity in scale sizes in respective investigations. It also remains unclear how energetic electrons behave,

given that the relevant observational analysis is rare (e.g., [23]). These are topics to be further pursued.

Acknowledgments
We are grateful to our colleagues at SPA/CSPAR, UAH, Drs. Laxman Adhikari, Gang Li, Gary Webb, Gary Zank, and Lingling Zhao for on-going collaborations. The in-situ spacecraft data are accessed via the Coordinate Data Analysis Web (CDAWeb) of NASA GSFC and the ACE Science Center. We acknowledge NASA grants NNX15AI65G, NNX17AB85G, 80NSSC18K0623, 80NSSC19K0276, and subaward SAO SV4-84017, and NSF grant AGS-1650854 for support. Special thanks also go to the SCOSTEP/VarSITI program for support of the development and maintenance of the on-line small-scale flux rope database at `http://fluxrope.info`.

References

[1] Moldwin M B, Phillips J L, Gosling J T, Scime E E, McComas D J, Bame S J, Balogh A and Forsyth R J 1995 *Journal of Geophysical Research: Space Physics* **100** 19903–19910 ISSN 2156-2202 URL `http://dx.doi.org/10.1029/95JA01123`
[2] Moldwin M B, Ford S, Lepping R, Slavin J and Szabo A 2000 *Journal of Geophysical Research: Space Physics* **27** 57–60
[3] Cartwright M L and Moldwin M B 2010 *Journal of Geophysical Research (Space Physics)* **115** A08102 ISSN 2156-2202 a08102 URL `http://dx.doi.org/10.1029/2009JA014271`
[4] Hu Q, Zheng J, Chen Y, le Roux J and Zhao L 2018 *Astrophys. J. Supp.* **239** 12 (*Preprint* `1810.01308`)
[5] Chen Y, Hu Q, le Roux J and Zheng J 2018 *Journal of Physics: Conference Series* **1100** 012006 URL `https://doi.org/10.1088/012006`
[6] Chen Y, Hu Q and le Roux J A 2019 *The Astrophysical Journal* **submitted** (*Preprint* `1905.00986`)
[7] Feng H Q, Zhao G Q and Wang J M 2015 *Journal of Geophysical Research: Space Physics* **120** 10,175–10,184 ISSN 2169-9402 2015JA021643 URL `http://dx.doi.org/10.1002/2015JA021643`
[8] Huang J, Liu Y C M, Peng J, Qi Z, Li H, Klecker B, Song H, Zheng J and Hu Q 2018 *Journal of Geophysical Research (Space Physics)* **123** 7167–7180
[9] Zhao L L, Zank G P, Chen Y, Hu Q, le Roux J A, Du S and Adhikari L 2019 *The Astrophysical Journal* **872** 4 URL `https://doi.org/10.3847/1538-4357/aafcb2`
[10] Hu Q 2017 *Sci. China Earth Sciences* **60** 1466–1494
[11] Zheng J and Hu Q 2018 *Astrophys. J. Lett.* **852** L23 (*Preprint* `1801.01771`)
[12] Zhou M, Bhat P, Loureiro N F and Uzdensky D A 2019 *arXiv e-prints* (*Preprint* `1901.02448`)
[13] Servidio S, Matthaeus W H and Dmitruk P 2008 *Physical Review Letters* **100** 095005
[14] Greco A, Matthaeus W H, Servidio S, Chuychai P and Dmitruk P 2009 *The Astrophysical Journal Letters* **691** L111 URL `http://stacks.iop.org/1538-4357/691/i=2/a=L111`
[15] Wan M, Matthaeus W H, Servidio S and Oughton S 2013 *Physics of Plasmas* **20** 042307
[16] Rappazzo A F and Parker E N 2013 *The Astrophysical Journal* **773** L2 URL `https://doi.org/10.1088/2041-8205/773/1/l2`
[17] Matthaeus W H, Bieber J W, Ruffolo D, Chuychai P and Minnie J 2007 *The Astrophysical Journal* **667** 956–962
[18] Zank G P, Adhikari L, Hunana P, Shiota D, Bruno R and Telloni D 2017 *The Astrophysical Journal* **835** 147 URL `http://stacks.iop.org/0004-637X/835/i=2/a=147`
[19] Drake J F, Swisdak M, Che H and Shay M A 2006 *Nature* **443** 553–556
[20] Hu Q, Smith C W, Ness N F and Skoug R M 2004 *Journal of Geophysical Research: Space Physics* **109** ISSN 2156-2202 a03102 URL `http://dx.doi.org/10.1029/2003JA010101`
[21] Hasegawa H, Sonnerup B U and Nakamura T K M 2010 *Journal of Geophysical Research: Space Physics* **115** (*Preprint* `https://agupubs.onlinelibrary.wiley.com/doi/pdf/10.1029/2010JA015679`) URL `https://agupubs.onlinelibrary.wiley.com/doi/abs/10.1029/2010JA015679`
[22] Du S, Guo F, Zank G P, Li X and Stanier A 2018 *The Astrophysical Journal* **867** 16 URL `https://doi.org/10.3847/1538-4357/aae30e`
[23] Chen L J, Bhattacharjee A, Puhl-Quinn P A, Yang H, Bessho N, Imada S, Mühlbachler S, Daly P W, Lefebvre B, Khotyaintsev Y, Vaivads A, Fazakerley A and Georgescu E 2008 *Nature Physics* **4** 19–23